A novel hyperspectral camera concept for SWIR-MWIR applications

A novel hyperspectral camera concept for SWIR-MWIR applications

Massimo Zucco, Marco Pisani and Domenico Mari
Istituto Nazionale di Ricerca Metrologica
INRIM
Torino, Italy
m.zucco@inrim.it

***Abstract*—We present the preliminary results of a hyperspectral imaging camera in the near medium infrared region (1.5 µm - 5 µm) of the electromagnetic spectrum. This region is important to undertake remote sensing by detecting pollutants released by industrial plants, or methane gas leaked by pipes, or even to study the efficiency and the gases produced by combustion reactions. The hyperspectral camera is based on a Fabry-Perot interferometer.**

Keywords—hyperspectral imaging; remote sensing; SWIR; MWIR;

I. INTRODUCTION

Hyperspectral imaging (HSI) is a combination of an imaging device (a digital camera) and a spectrophotometer. The obtained data set, known as "hyperspectral cube" or "hypercube", is a three dimensional matrix formed by a 2D image combined with a third dimension that is the spectral composition of each pixel of the image. There are an increasing number of applications of HSI devices in different fields of physics; to name but a few in thermal imaging [1], in fluorescence microscopy [2], in remote sensing of pollutant gases [3], in space missions, like in the Rosetta mission the VIRTIS camera used to take hyperspectral images of comet Churyumov-Gerasimenko [4], or in cultural heritage [5].

There are basically three different techniques of HSI. The first technique is obtained by integrating a dispersive means (a prism or a grating) in an optical system. In this HSI the image is analyzed per lines and the scan is obtained with some mechanics integrated in the optical train. The second HSI technique is based on optical filters with tunable or fixed band-pass and the spectrum has to be acquired by scanning the steps in frequency. Finally the third method to obtain the spectra of an image is based on the so called Fourier transform (FT) spectroscopy; here the FT is applied to the interferogram acquired by a scanning interferometer. There are two intrinsic advantages in using interferometer-based spectrometers, one is called multiplex of Fellgett advantage when the noise is dominated by detector noise: the information at all the wavelengths is collected simultaneously and the improvement of the signal to noise ratio is proportional to the square root of the number of bins. According to the second advantage, called Jacquinot advantage, the optical throughput of FT spectroscopy is intrinsically higher than dispersive HSI because there are no slits that are used in dispersive means to define the wavelength resolution.

Atmospheric gases and pollutants have important absorption bands in the infrared region. According to the DIN standardization the band of interest is divided in SWIR (1.4 µm – 3 µm), in the MWIR (3 µm – 8 µm) and in the LWIR (8 µm – 15 µm). Hyperspectral imaging in this range could be implemented to undertake remote sensing by detecting pollutants released by industrial plants, or methane gas leaked by pipes, or even to study the efficiency and the gases produced by combustion reactions without coming into physical contact. Moreover, hyperspectral imaging in the IR could be used to carry out thermography by measuring the blackbody radiation emitted by surfaces.

Hyperspectral imagers in the SWIR, MIR region based on Michelson interferometers are produced and commercialized by Bruker [6] and by Telops [7] reaching spectral resolution below cm^{-1} and spatial resolutions dependent on the implemented optics. They have found applications in detection of methane emissions from a shallow lake scene [8] or measurement of ethylene and ammonia emissions from different sources of an industrial area [9].

II. TOWARDS A NEW PROTOTYPE

We plan to extend the range of our prototype of hyperspectral imager which was realized and validated in the UV-VIS-NIR bands [10] to the 1.5 µm – 5 µm band which are part of the SWIR and MWIR bands. Differently from the commercial systems, it is based on a Fabry-Perot interferometer. The spectral information for each pixel is (F-P) recorded in the interferogram acquired while scanning the optical path delay between the mirrors with piezo actuators. The spectra for each pixel are then calculated using a Fourier transform based algorithm. A basic set-up is presented in Fig. 1 where the optical system is formed by the photographic objective, on the right hand side, that forms the image on the CCD camera on the left hand side. In between, the F-P interferometer formed by two semi-reflective metallic mirrors where the distance is varied in this prototype by means of three PZT actuators. While the optical path distance is varied, a video is acquired and the interferograms for each pixel are recorded in the video. The calibration of the retardation is

obtained for each pixel by using a laser radiation of known wavelength that is superimposed to the image.

Fig. 1. The optical set-up formed by a photographic objective, on the right hand side, that forms the image of the scene on the CCD camera on the left hand side. In the middle the F-P interferometer. The three piezo actuators that change the optical path distance by moving the mirrors are visible in the aluminum structure.

This working prototype cannot be automatically used to work in the 1.5 µm – 5 µm band for the following technical limitations:

- The core of the hyperspectral imager prototype is the Fabry-Perot interferometer which is formed by two semi-reflective mirrors (beam splitters) having a reflectance of about 20-30%, coated either with dielectric or metallic layers [11]. The substrate material is a BK7 or fused silica which cuts for wavelengths longer than about 2 µm and therefore opaque in the IR region of interest.

- The responsivity of the CCD and CMOS camera based on silicon goes between 300 nm to 1100 nm, the responsivity of the CCD and CMOS camera based on InGaAs ranges from 900 nm to 1700 nm

- The transmissivity of the commercial photographic objectives, used to form the image on the camera, reaches zero value for wavelength longer than about 2 µm

- The spectral resolution of the prototype is limited to 100 cm^{-1} as a consequence of the maximal mirror distance (40 µm) attainable with three amplified piezo actuators with flexure stages.

For the technical details reported above, the extension of the hyperspectral imager to the IR, and in particular in the region of interest 1.5 µm – 5 µm, requires completely new technical solutions.

III. Realization of a New Prototype

For the realization of our prototype in the infrared we adopted the following solutions. Regarding the beam splitters since there are no pairs of semi reflective mirrors with the required reflectivity of about 20%-30% in the region 1.5 µm – 5 µm available on the market, we considered to use silicon as dielectric substrate which has the relative transmission reported in Fig 2 for a thickness of 5 mm.

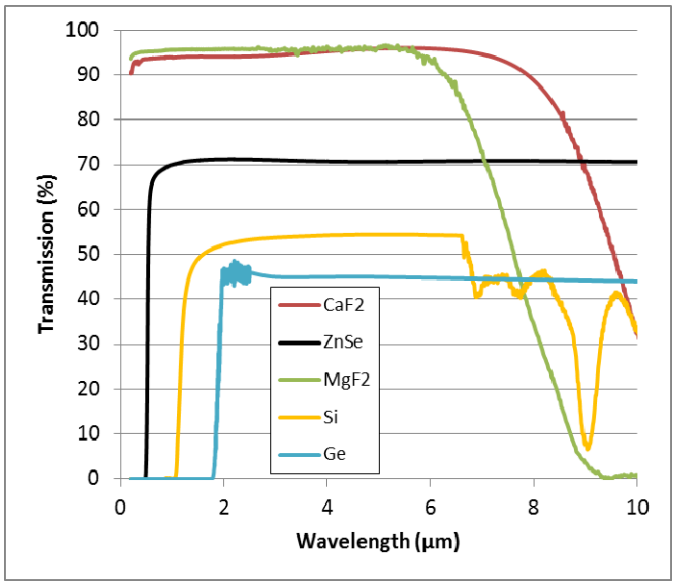

Fig. 2. Transmission of different materials in the infrared region for a thickness of 5 mm.

Silicon, like Zinc Selenide, has an index of refraction sufficiently high (*n*, about 2.5-3.5) to have a reflectance, calculated with Fresnel formula, at the required level (*R*, about 20%-30%) and in this case there is no need of applying a coating to increase the reflectance, see Fig 3.

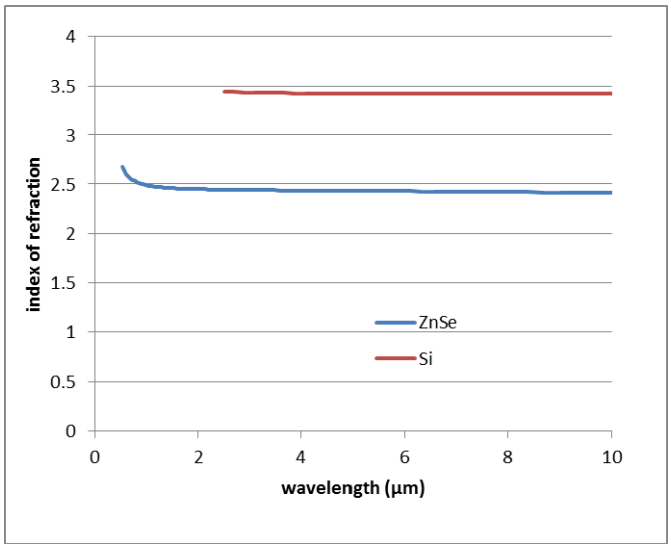

Fig. 3. Index of refraction in the infrared for Silicon and Zinc Selenide

The Fabry-Perot is finally realized with a pair of silicon wafers with a diameter of 3 inches lapped on both faces. The two are inserted in a sealed frame and the distance between the mirrors, in order to have a scan of the optical path delay, was obtained with a pneumatic system as described in [11] and presented in Fig 4.

Fig. 4. The Fabry-Perot interferometer formed by two silicon wafers inserted in a sealed structure where the distance is varied with a pneumatic technique.

A preliminary test of the system was carried out with the set-up presented in Fig 5 where the light from a filament lamp (at the top of the figure) is coupled into the monocromator. The monocromator is set in order to have at the output a radiation at 3.5 µm, The output slit width is set at 1 mm.

The Fabry-Perot interferometer is positioned just in front of the infrared camera. We have used two types of infrared cameras, a Xenics XS Base, XC117B (0.9 µm – 1.7 µm), and a FLIR A6750sc MWIR (3 µm – 5 µm).

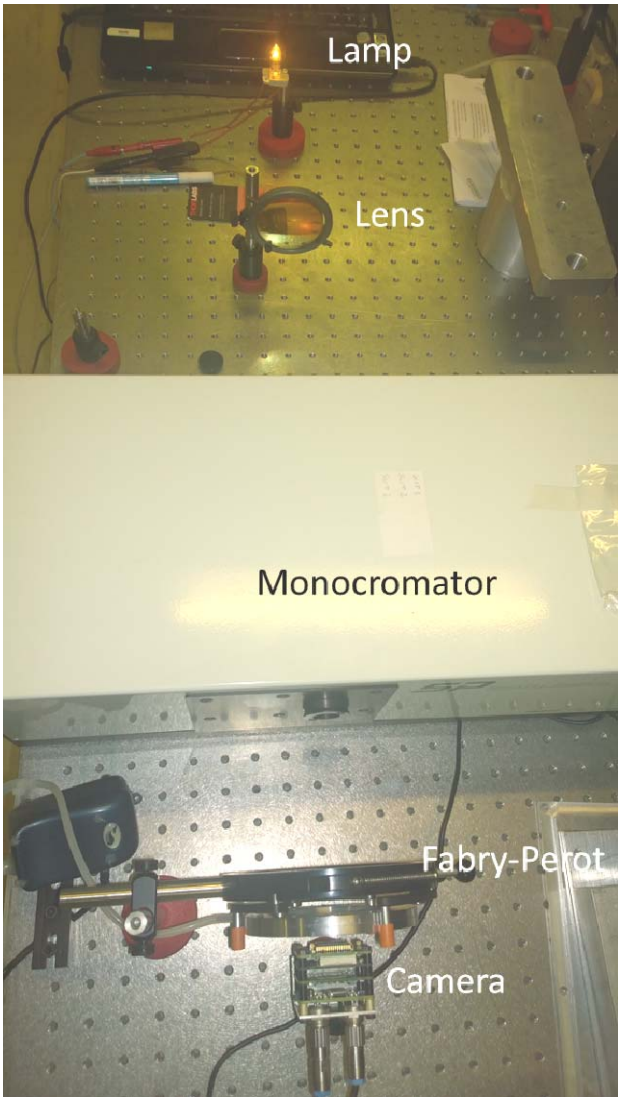

Fig. 5. Set-up to test the Fabry-Perot in the infrared region. At the top the filament lamp, in the center the monocromator and at the bottom the Fabry-Perot interferometer in front of the camera.

The preliminary results are obtained with the FLIR camera. A video is recorded while the mirror distance is varied. In Fig 6 is presented an image extracted from the video where the grey levels represent the counts for each pixel, the bit depth is 14 bits. In the center of the image, the rectangular region is the output of the monocromator set at 3.5 µm. The rest of the image is darker because the surface of the scene emits like a blackbody at the ambient temperature of the laboratory.

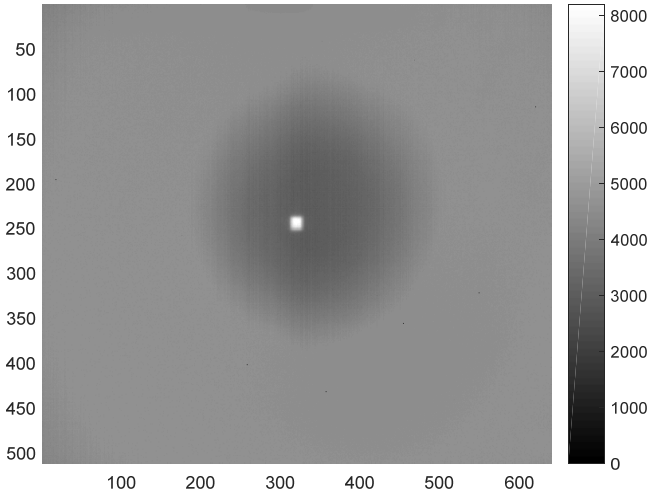

Fig. 6. Image extracted from the video where the grey levels represent the counts for each pixel, the bit depth is 14 bits..

In Fig 7 the zoom of Fig 6 with the two regions used for the test. From the succession of the frames of the video the interferogram for each pixel is extracted. In Fig. 8 the interferogram of the pixel of the radiation coming from the monocromator indicated with the red arrow in Fig 7.

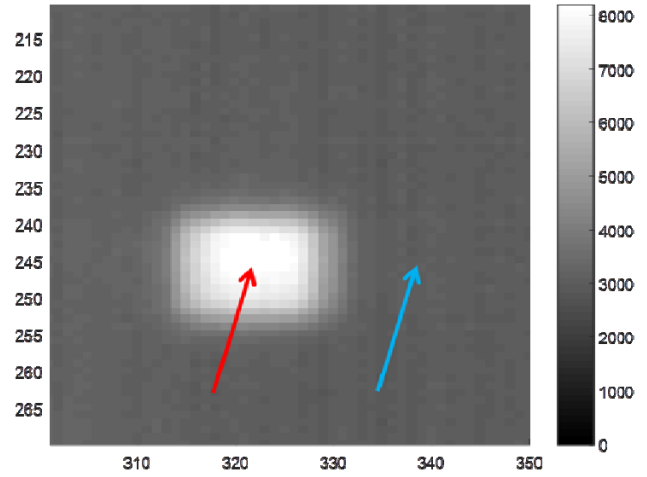

Fig. 7. Image extracted from the video where the grey levels represent the counts for each pixel, the bit depth is 14 bits. The arrows indicate the regions used for the test.

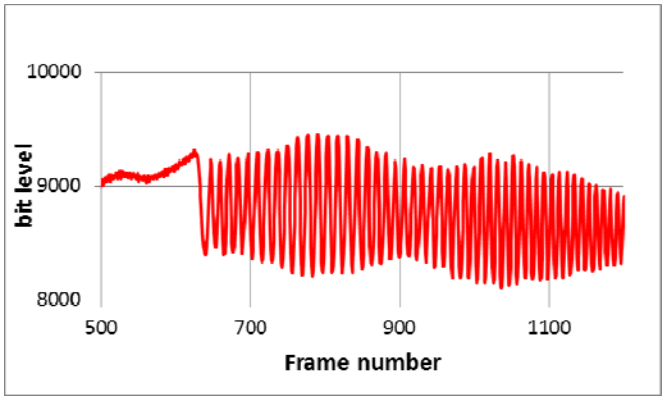

Fig. 8. Interferogram of the pixel in the scene of the radiation coming from the monocromator indicated by a red arrow in Fig. 7.

In Fig. 9 the interferogram of the region indicated with the blue arrow in Fig 7.

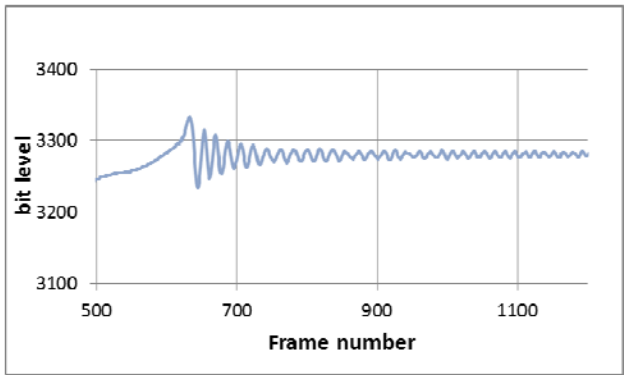

Fig. 9. Interferogram of the pixel in the scene indicated by a blue arrow in Fig. 7.

The interferogram in Figure 8 is used to calibrate the mirror displacement since the radiation is monocratic and the fringe corresponds to a displacement of half the wavelength, i.e. 1.75 µm. With this calibration we have calculated the spectrum of the interferogram in Fig 9 with an algorithm based on the Fourier transform, and reported in blue in Fig 10. The red curve in Fig 10 represents the spectrum of another pixel of the radiation coming from the monocromator at 3.5 µm.

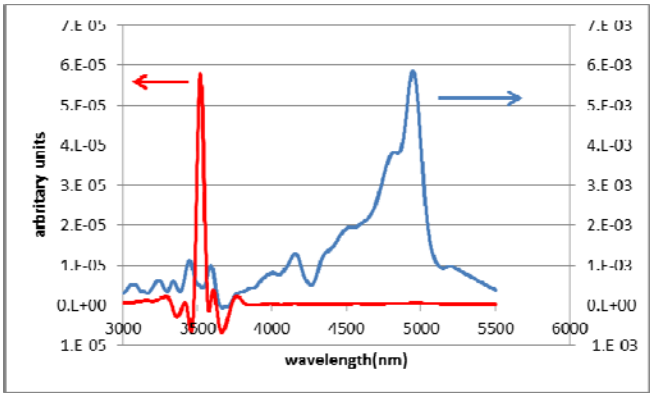

Fig. 10. The blue curve is the spectrum of the region indicated by the blue arrow in Fig 7. The red curve is the spectrum of a different pixel of the radiation at 3.2 µm.

In Fig 11 the same spectra as in Fig. 10 but represented in frequency over a broader region in order to show the harmonic of the spectra coming from the algorithm.

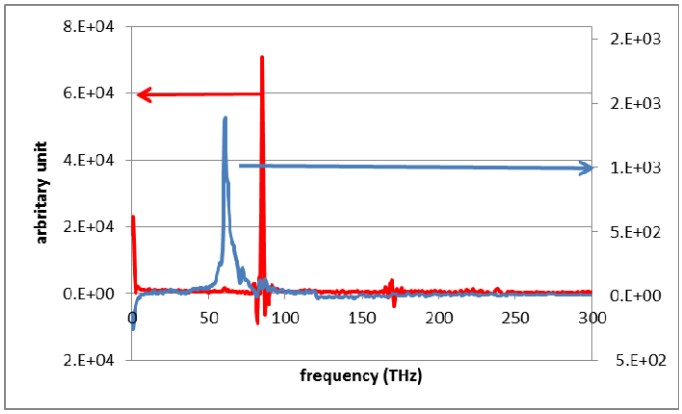

Fig. 11. The blue curve is the spectrum of the region indicated by the blue arrow in Fig 7. The red curve is the spectrum of a different pixel of the radiation at 3.2 µm.

IV. Conclusions

The preliminary results show that a hyperspectral camera based on a Fabry-Perot interferometer with the semi reflective mirrors formed by silicon substrate which work in the infrared region is possible. The pneumatic actuator ensures the variation of the optical path difference. The spectra are calculated from the interferogram extracted from the video.

Acknowledgments

The authors would like to thank Raphaël Danjoux and Francesco Messa from FLIR for support.

References

[1] M. Pisani, P. Bianco, M. Zucco, “Hyperspectral imaging for thermal analysis and remote gas sensing in the short wave infrared”. Applied Physics B, Laser ans Optics, vol 108 (1), pp. 231-236, 2012

[2] M Pisani, M Zucco “Fabry–Perot-based Fourier-transform hyperspectral imaging allows multi-labeled fluorescence analysis” Appl. Optics, vol. 53, pp. 2983-2987, 2014.

[3] R. Harig, A. Keens, P. Rusch, J. Gerhard, S. Sabbah, “Hyperspectral sensor for analysis of gases in the atmosphere (HYGAS)”. Proc. SPIE 7695, Algorithms and Technologies for Multispectral, Hyperspectral, and Ultraspectral Imagery XVI, 76950B (May 12, 2010);

[4] A. Coradini, F. Capaccioni, P. Drossart, G. Arnold, E. Ammannito, F. Angrilli, A. Barucci, G. Bellucci, J. Benkhoff, G. Bianchini, JP. Bibring, “VIRTIS: An imaging spectrometer for the Rosetta mission”, Space Science Reviews. 2007 Feb 1;128(1-4):529-59.

[5] M. Zucco, M. Pisani and T. Cavaleri , “Fourier Transform Hyperspectral Imaging for Cultural Heritage” in Fourier Transforms - High-tech Application and Current Trends, Prof. Goran Nikolić (Ed.), InTech, DOI: 10.5772/66107. Available from: http://www.intechopen.com/books/fourier-transforms-high-tech-application-and-current-trends/fourier-transform-hyperspectral-imaging-for-cultural-heritage

[6] https://www.bruker.com

[7] http://www.telops.com

[8] M. Gålfalk, G. Olofsson, P. Crill, and D. Bastviken, “Making methane visible”. *Nature Climate Change*, *6*(4), 426-430, 2016

[9] S. Sabbah, P. Rusch, J.-H. Gerhard, C. Stöckling, J. Eichmann and R. Harig, “Remote sensing of gases by hyperspectral imaging: results of measurements in the Hamburg port area”, Proc. SPIE 8186, Electro-Optical Remote Sensing, Photonic Technologies, and Applications V, 81860S (October 05, 2011); doi:10.1117/12.899687.

[10] M. Pisani and M. E. Zucco, “Compact imaging spectrometer combining Fourier-transform spectroscopy with a Fabry–Perot interferometer,” Opt. Express, vol. 17, pp. 8319–8331, 2009.

[11] M. Zucco, M. Pisani, V. Caricato, and A. Egidi, “A hyperspectral imager based on a Fabry-Perot interferometer with dielectric mirrors”, Opt. Express, vol. 22(2), pp. 1824-34, 2014.

[12] V. Caricato, A. Egidi, M. Pisani, M. Zucco, and M. Zangirolami. "A device for hyperspectral imaging in the UV." In Precision Electromagnetic Measurements (CPEM 2014), 2014 Conference on, pp. 706-707. IEEE, 2014.